inhibiting epithelial cadherin (E-cadherin; encoded by *CDH1*) expression and acquiring mesenchymal markers. This process is physiologically important during embryogenesis and is required for in utero development. Given that PKM2 expression and EMT are common to both tumorigenesis and development, PKM2 may affect EMT within cancer cells. However, the significance of PKM2 during EMT or invasion is yet to be investigated.

In the present study, we demonstrate that PKM2 translocates into the nucleus during EMT and acts as a transcription cofactor that inhibits *CDH1* expression. PKM2 interacts with TGF-β–induced factor homeobox 2 (TGIF2), which recruits histone deacetylase 3 (HDAC3) to the promoter sequence of E-cadherin, thereby promoting histone H3 lysine 9 (H3K9) deacetylation and *CDH1* expression down-regulation.

Results

EMT Induction Elicits Nuclear Translocation of PKM2. For the induction of EMT, we cultured colon cancer cells in a medium with TGF-β1 and EGF, as described previously (Fig. 1*A*) (11–14). The SW480 cells changed morphology from epithelial to fibroblastic-like and spindle-shaped in a time-dependent manner (Fig. 1*B*). Consistent with this observation, *CDH1* transcript expression was suppressed, whereas the expression levels of the vimentin (*VIM*), zinc finger e-box binding homeobox 1 (*ZEB1*), and snail family zinc finger 2 (*SNAI2*) genes were increased (Fig. 1*C*). PK gene expression was induced in the EMT condition, with preferential expression of PKM2 compared with PKM1 (Fig. 1*D*). Western blot analysis indicated that the induction of EMT resulted in decreased *CDH1* expression, increased *VIM* expression, and up-regulated PKM2 (Fig. 1*E*). We confirmed that the expression and secretion of endogenous TGF-β1 was minimal in SW480 (Fig. S1 *A* and *B*).

To determine the intracellular localization of proteins, cytoplasmic and nuclear fractions were separated from the EMT-induced cells and Western blot analysis was performed. The data indicated that, although the EMT condition stimulated an increase in cytoplasmic PKM2, nuclear PKM2 was augmented compared with levels in the pre-EMT state (Fig. 1*F*). Immunocytochemistry and immunofluorescence intensity quantification confirmed the increase in nuclear PKM2 (Fig. S2 *A*–*D*). In addition, we confirmed that nuclear PKM2 was also increased in HCT116 cells under the same EMT condition (Fig. S2*E*) and that the expression of EMT markers was increased in murine *Pkm2* knock-in, compared with *Pkm1* knock-in, mesencymal cells, as well as other human cancer cells (Fig. S1 *C* and *D*).

Previous studies showed that EGF stimulation increased nuclear PKM2 (7) and indicated that cytoplasmic PKM2 functions with tetramer formation, whereas nuclear PKM2 functions with dimer formation. Given that the large hydrophobic hole at the nucleotide binding site is buried in tetrameric PKM2 structure, which becomes accessible in dimer form (15), the dimer formation may provide a protein binding ability. We studied the status of PKM2 during EMT and found that simultaneous stimulation by TGF-β1 and EGF, in comparison with either alone, resulted in increased expression of an ~120-kDa complex, corresponding to dimeric PKM2 (Fig. 1*G* and Fig. S3). The present study demonstrated that PKM2 nuclear translocation was stimulated in the EMT condition, suggesting a unique function of PKM2 in the nucleus.

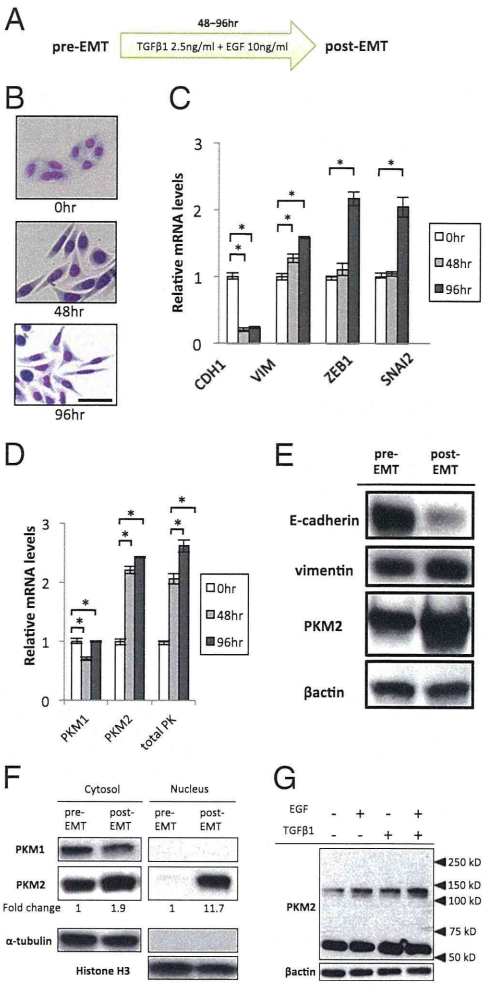

Fig. 1. PKM2 translocates into the nucleus during EMT. (*A*) Schematic representation of the procedure for EMT induction. The cells incubated for 48 h after seeding are defined as pre-EMT, and the cells cultured with 2.5 ng/mL TGF-β1 and 10 ng/mL EGF are defined as post-EMT. (*B*) Photomicrographs of the morphological change in SW480 cells. The cells were stained using the Diff-Quik Kit (Sysmex Corp.). The number of hours indicates the period since EMT induction was initiated. (Scale bar, 100 μm.) (*C*) Relative transcript (mRNA) levels of *CDH1*, *VIM*, *ZEB1*, and *SNAI2* after induction of EMT for 0, 48, and 96 h. The values at 0 h (pre-EMT) have been normalized to 1, and the data are expressed as fold. (*D*) Relative mRNA levels of PKM1, PKM2, and pyruvate kinase (total PK) after induction of EMT for 0, 48, and 96 h. (*E*) Western blot assays of E-cadherin, vimentin, and PKM2 expression in pre-EMT and post-EMT cells. Post-EMT cells were harvested at 72 h. (*F*) Western blot assays of PKM1, PKM2, α-tubulin, and histone H3 in nuclear and cytoplasmic lysates prepared from SW480 cells. With normalization to cytoplasmic tubulin or nuclear histone H3 blots, the relative intensities of PKM2 blots are shown in comparison with those in the pre-EMT condition. (*G*) SW480 cells were treated with dimethyl suberimidate for 30–60 min, immediately followed by whole cell lysis. The monomer and dimer states of PKM2 were analyzed by Western blot assay. Columns represent the average of at least three independent experiments; error bars represent the SD of the mean from triplicate results. $*P < 0.05$.

PKM2 Expression Is Required to Induce EMT. To investigate the causative role of PKM2 in EMT induction, we cultured cells with endogenous PKM2 inhibition by small interfering RNA (siRNA) knockdown (KD) under EMT conditions. We used the siRNA targeting system, which reportedly inhibits PKM2 without any off-target effects on other genes (16), and the results indicate that the most effective siRNA sequence could inhibit transcriptional and translational levels of PKM2, whereas those of PKM1 were increased (Fig. S4 *A* and *B*). PKM2 KD failed to induce spindle-shaped morphological changes under EMT conditions (Fig. 2*A*). Expression analysis indicated that PKM2 KD prevented *CDH1* down-regulation, although *VIM* expression persisted (Fig. 2*B*), suggesting a role for PKM2 in *CDH1* transcription. Fifty percent reductions in glucose or glutamine in the medium did not have significant effects on EMT marker expression (Fig. S5*A*), suggesting distinct effects on EMT and metabolism.

Western blot analysis indicated that PKM2 KD hindered *CDH1* loss and *VIM* gain compared with the control (Fig. 2*C*).

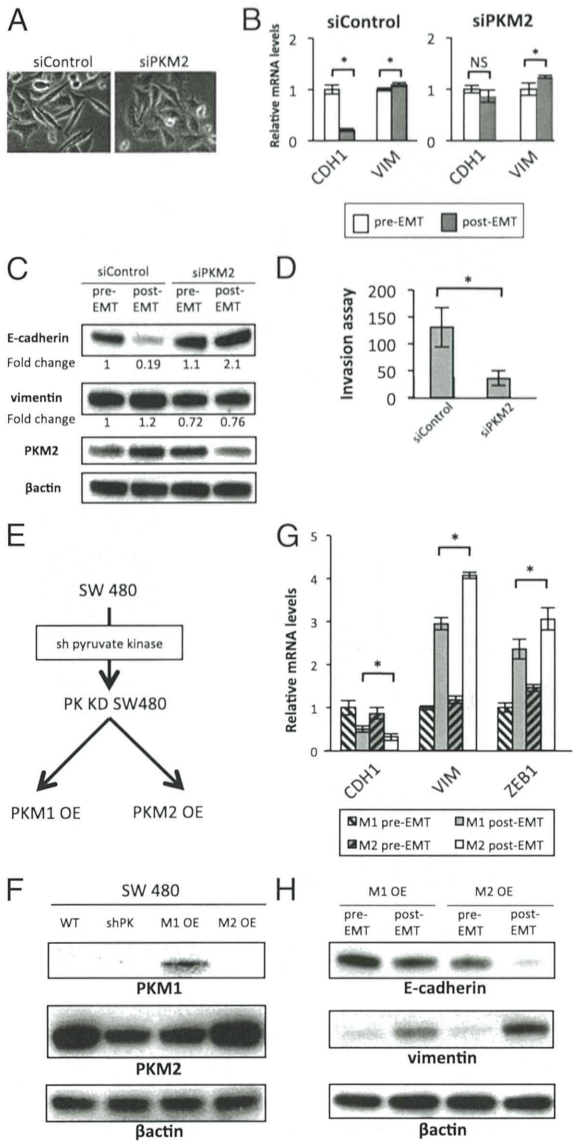

Fig. 2. PKM2 is required for EMT induction. (*A*) Phase-contrast photomicrographs of SW480 cells transfected with siControl or siPKM2 after EMT induction for 48 h. (*B*) Relative transcript (mRNA) levels of *CDH1* and *VIM* after EMT induction in cells transfected with siControl or siPKM2 for 48 h. (*C*) Western blot assays of E-cadherin, vimentin, PKM2, and β-actin expression in pre-EMT and post-EMT cells. Post-EMT cell samples were harvested at 72 h. With normalization to β-actin as a control, the relative intensities of E-cadherin and vimentin are shown in comparison with those in the control pre-EMT condition. Note that siPKM2 knockdown works efficiently in post-EMT cells. (*D*) Invasive behavior of SW480 cells treated with siControl or siPKM2. (*E*) Schematic procedure for establishing PKM1 OE or PKM2 OE SW480 cells. (*F*) Western blot assays of PKM1, PKM2, and β-actin expression in WT SW480 cells, cells stably expressing shRNA constructs targeting pyruvate kinase (shPK), and shPK cells overexpressing either PKM1 or PKM2 constructs. (*G*) Relative mRNA levels of *CDH1*, *VIM*, and *ZEB1* after EMT induction in PKM1 OE or PKM2 OE SW480 cells for 72 h. (*H*) Western blot assays of E-cadherin, vimentin, and β-actin expression in PKM1 OE and PKM2 OE cells. Post-EMT cell samples were harvested at 72 h. Column values = average of at least three independent experiments; error bars represent SD from the mean of triplicate experiments. $*P < 0.05$.

Inhibition of EMT by PKM2 KD resulted in a significant reduction in in vitro cellular invasiveness (Fig. 2*D*). The assessment of mothers against decapentaplegic homolog 2 (SMAD2) and ERK, which are downstream effectors of TGF-β1 and EGF signaling, indicated that PKM2 KD disturbed the phosphorylation process (Fig. S5*B*).

To minimize the effect of an alternative exon and to focus on the function of PKM2 in the nucleus, we established PKM1- and PKM2-overexpressing (OE) cell lines (PKM1 and PKM2 OE in Fig. 2*E*). In brief, we transfected the cells with a small hairpin RNA (shRNA) vector targeting the common region in *PK* and then introduced an overexpression vector of PKM1 or PKM2 cDNA without a complementary sequence to the shRNA (Fig. 2*F*). We cultured the established cells in EMT-inducing conditions. The results demonstrated a greater decrease in *CDH1* expression and greater increase in *VIM* and *ZEB1* expression in PKM2 OE cells compared with that in PKM1 OE cells (Fig. 2*G* and Fig. S4*C*). Consistent results were obtained by Western blot analysis (Fig. 2*H*). These results indicate that PKM2 expression is necessary for EMT induction.

Nuclear PKM2 Binds to TGIF2 and Represses CHD1 Expression. Nuclear PKM2 reportedly binds to and phosphorylates STAT3 through its function as a protein kinase (15). The observation that nuclear PKM2 increased during EMT led us to consider the possibility that PKM2 may interact with other transcription factors. To validate this hypothesis, fractions pulled-down with the PKM2 antibody were subjected to LC-electrospray ionized TOF MS analyses. The result showed that nuclear PKM2 was coimmunoprecipitated with TGIF2 and that this binding was detectable when both EGF and TGFβ1 were added to the culture (Fig. 3*A*). These findings were confirmed by immunoprecipitation, followed by Western blot analysis (Fig. 3*B*). The EMT stimulation resulted in the significant increase of TGIF2 expression (Fig. S6*A*). TGIF2 KD did not show significant alterations of PKM2 expression regardless of EMT induction (Fig. 3*E* and Fig. S6*B*). We could not detect an association of PKM1 with TGIF2 in the nucleus (Fig. S7*A*), which further supports the cytoplasmic localization of PKM1 (Fig. 1*F*).

Melhuish et al. (17) revealed that TGIF2 is a transcriptional repressor that suppresses TGF-β–responsive gene expression by binding to TGF-β–activated SMADs. First, we performed TGIF2 KD, followed by EMT induction (Fig. 3*C* and Fig. S6*B*). TGIF2 KD enhanced the decrease in both the transcriptional and the translational levels of *CDH1* expression (Fig. 3 *D* and *E*). To analyze the difference in the effect of TGIF2 KD in cells expressing either PKM1 or PKM2, we performed TGIF2 KD on PKM1 OE and PKM2 OE cells, followed by EMT induction. Interestingly, the decrease in *CDH1* expression and increase in *VIM* expression were similar at the transcriptional and translational levels after EMT induction in both cell lines (Fig. 3 *F* and *G*). These results indicate that the augmented sensitivity to EMT induction in PKM2 OE cells is abrogated under TGIF2 suppression. These data further suggest that nuclear PKM2 responds to EMT stimulation and interacts with TGIF2 to mediate EMT induction downstream of PKM2.

PKM2 and TGIF2 Recruit HDAC3 to the *CDH1* Promoter to Repress Transcription. TGIF2 is a transcriptional factor that regulates TGF-β signal transduction (17). Based on the above findings, we hypothesized that TGIF2 could bind to the *CDH1* promoter and activate *CDH1* expression in the epithelial state. To examine this hypothesis, we performed a ChIP quantitative PCR (qPCR) assay using two sets of primers located in the *CDH1* promoter sequence region (Fig. 4*A*). We found depressed binding of TGIF2 to the *CDH1* promoter region during EMT (Fig. 4*B*).

TGIF2 can control transcription by recruiting HDAC in response to TGF-β signaling (17) and PKM2 can associate with HDAC3 in the nucleus (7). To investigate whether TGIF2 can bind to HDAC3 during EMT, we performed immunoprecipitation followed by Western blot analysis and found an association between TGIF2 and HDAC3 under EMT induction (Fig. 4*C* and

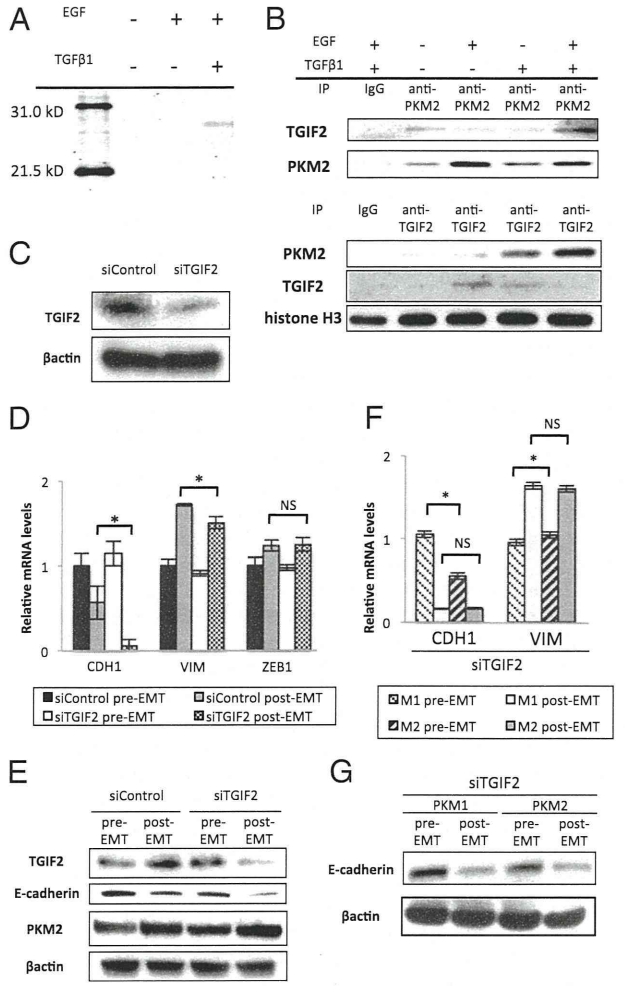

Fig. 3. Interaction between nuclear PKM2 and TGIF2 mediates EMT induction. (*A*) Polyacrylamide gel electrophoresis of proteins immunoprecipitated with anti-PKM2 antibody in the nucleic lysate of cells cultured under normal conditions, with EGF alone, or with TGF-β1 and EGF. The band detected in samples of cells stimulated with TGF-β1 and EGF was excised and analyzed by MS. (*B*) Western blot assays of immunoprecipitated samples of nucleic lysates with anti-PKM2 or anti-TGIF2 antibody. Samples were harvested after the cells were treated as indicated for 72 h. (*C*) Western blot assays of TGIF2 and β-actin expression in cells transfected with siControl or siTGIF2. (*D*) Relative transcript (mRNA) levels of *CDH1*, *VIM*, and *ZEB1* after induction of EMT in cells transfected with siControl or siTGIF2 for 72 h. (*E*) Western blot analysis of TGIF2, E-cadherin, PKM2, and β-actin expression in pre-EMT and post-EMT cells transfected with siControl or siTGIF2. Post-EMT samples were harvested at 72 h, when siRNA inhibition was profound. (*F*) Relative mRNA levels of *CDH1* and *VIM* after EMT induction in PKM1 OE and PKM2 OE cells. Post-EMT samples were harvested at 72 h. (*G*) Western blot analysis of E-cadherin and β-actin after EMT induction in PKM1 OE and PKM2 OE cells transfected with siTGIF2. Post-EMT samples were harvested at 72 h. Column values = average of at least three independent experiments; error bars represent SD from the mean of triplicate experiments. $^*P < 0.05$.

Figs. S7*B* and S8). To examine the acetylation status of histone H3 in the *CDH1* promoter region, we performed ChIP qPCR and found that binding of acetylated H3K9 to the *CDH1* promoter was decreased under EMT conditions (Fig. 4*D*). Furthermore, to understand how the PKM2–TGIF2–HDAC3 complex can bind to the *CDH1* promoter, additional ChIP qPCR analysis was performed. The data indicated that similar to the binding of TGIF2, the binding of PKM2 and HDAC3 to the *CDH1* promoter was reduced during EMT (Fig. S9 *A* and *B*). Given that the TGIF2 protein bound to PKM2 and HDAC3 during EMT (Figs. 3*B* and 4*C* and Fig. S7*B*), the present study demonstrates that nuclear PKM2 plays a role in the TGIF2-dependent control of CHD1 expression and that EGF induces formation of the PKM2–TGIF2–HDAC3 complex, followed by histone deacetylation, thus resulting in suppressed *CDH1* expression. TGF-β1 may modulate the association of this complex, although H3K9 was deacetylated (Fig. 5*D*).

PKM2 Expression in the Deepest Tumor Regions Correlated with CRC Metastasis. To investigate the clinical significance of PKM2 expression in cancer metastasis, we immunohistochemically analyzed clinical CRC samples. Staining was assessed in the deepest tumor regions where the CRC invasion begins (18, 19). The

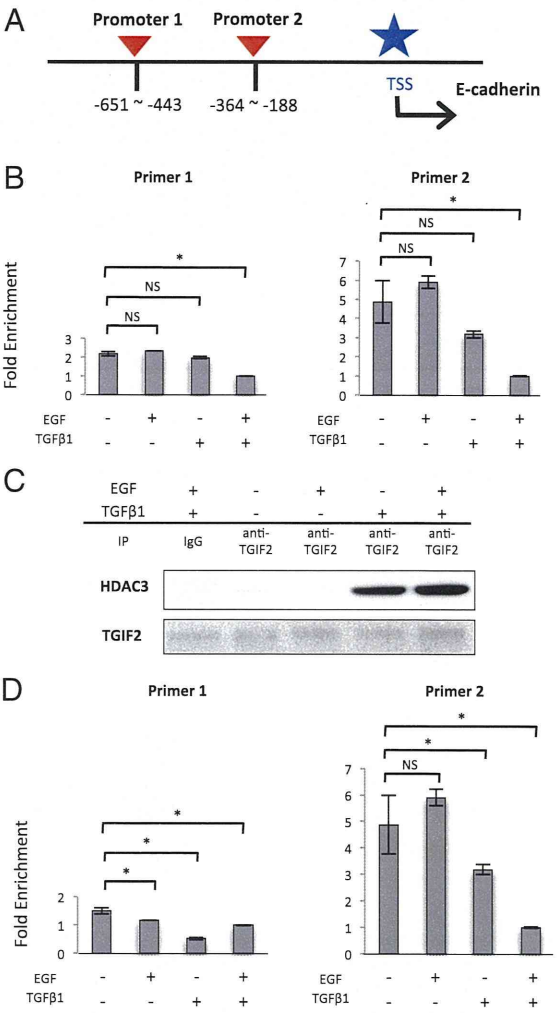

Fig. 4. TGIF2 binds to the CDH promoter and recruits HDAC3 during EMT. (*A*) Schematic diagram showing the positions of two sets of primers designed to cover the promoter region of the *CDH1* gene. (*B*) ChIP assays were performed with IgG and anti-TGIF2 antibody, followed by qPCR (mean ± SD, $n = 3$). ChIP samples were harvested from the nucleic lysate of SW480 cells treated as indicated for 72 h. (*C*) Western blot assays of immunoprecipitated samples of nucleic lysate with anti-TGIF2 antibody. Each sample was harvested after the cells were treated as indicated for 72 h. (*D*) ChIP assays were performed with IgG and anti-acetylated H3K9 antibody, followed by qPCR (mean ± SD, $n = 3$). ChIP samples were harvested from the nucleic lysate of SW480 cells treated as indicated for 72 h. Column values = average of at least three independent experiments; error bars represent SD from the mean of triplicate experiments. $^*P < 0.05$.

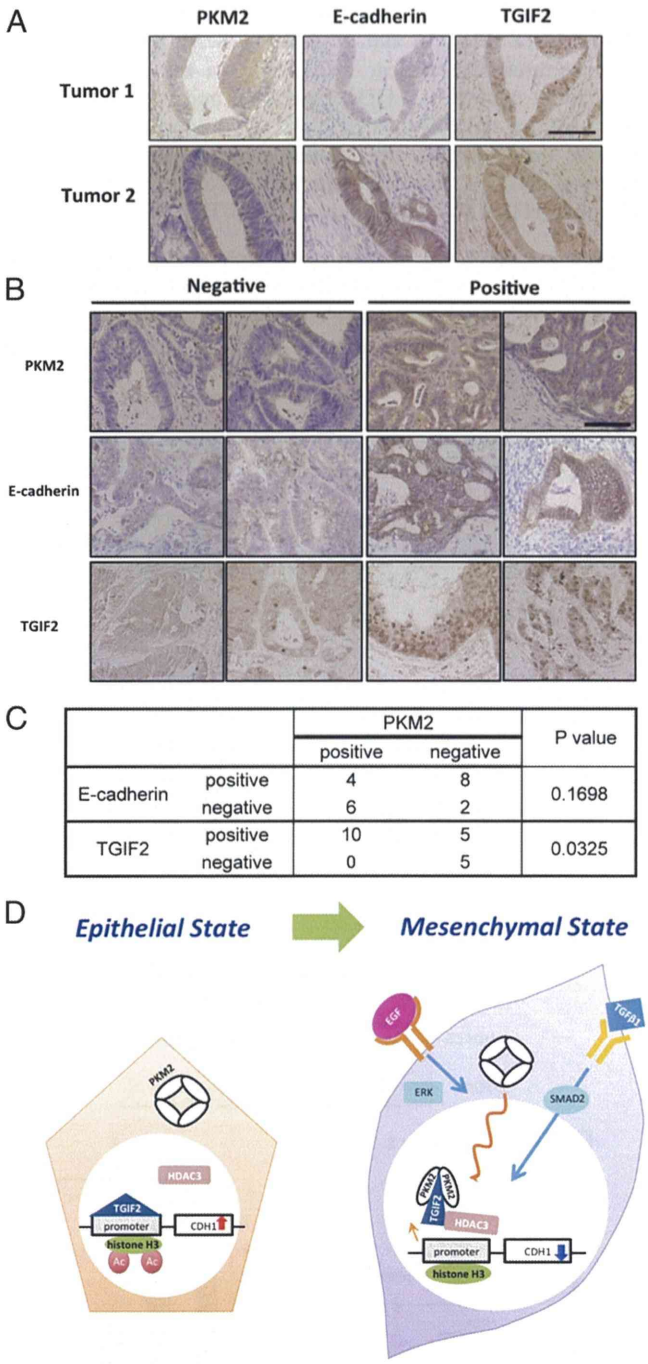

		PKM2 positive	PKM2 negative	P value
E-cadherin	positive	4	8	0.1698
	negative	6	2	
TGIF2	positive	10	5	0.0325
	negative	0	5	

Fig. 5. The immunohistochemistry. (*A*) Staining at the invasive front, showing an inverse correlation between PKM2, E-cadherin, and TGIF2 expression. (Scale bar, 100 μm.) (*B*) The representative cases are shown for staining for PKM2, TGIF2, and E-cadherin. Invasive fronts of tumors were stained by anti-PKM2, anti-E-cadherin, and anti-TGIF2 antibodies, and the intensities were assigned to positive and negative groups. With regard to TGIF2 staining, under the microscopic observation, cases with more than 50% of cells stained in nucleus were designated as positive, whereas the others were negative. (*C*) The 10 positive and 10 negative cases for cellular PKM2 were examined for nuclear TGIF2 and membranous E-cadherin. (*D*) Theoretical model illustrating the functional roles of PKM2 and TGIF2 in regulating *CDH1* transcription during EMT.

PKM2 staining intensities were assigned to positive and negative groups (Fig. 5 *A*–*C*). The correlations between PKM2 expression and clinicopathological factors are summarized in Table S1. PKM2-positive staining was significantly correlated with metastasis to lymph nodes and distant organs. To further understand the clinical significance of PKM2 in CRC, we analyzed the GSE17536 database of the gene expression array and patient prognosis. To study the specific effect of PKM2 in the array database, we analyzed expression of both PK and its splicing factor hnRNPA2, because hnRNPA2 stimulates the splicing to PKM2 (20, 21). As expected, cases with high PK and high hnRNPA2 expression showed a poorer prognosis than other groups; the difference in prognosis was apparent in stages III and IV with metastasis (Fig. S10 *A* and *B*). The data confirmed that PKM2 can enhance the ability of cancer cells to metastasize in primary cancer tissues.

Discussion

In the present study, we demonstrated that nuclear PKM2 interacts with TGIF2 during EMT, which is pivotal in promoting the transition into the mesenchymal cancer cell phenotype. Consequently, we propose a model for the nuclear PKM2 function in response to EMT stimulation (Fig. 5*D*). Under epithelial conditions, histone H3 is acetylated on the *CDH1* promoter region and *CDH1* is transcribed where TGIF2 should serve as an active transcription factor. Once the EMT signal stimulates transformation of the cancer cell, a PKM2 fraction enters the nucleus and associates with TGIF2. We assume that this association will alter the conformation of TGIF2 or its associated complexes, effectively loosening the binding between TGIF2 and the *CDH1* promoter sequence to allow the recruitment of HDAC3 and subsequent histone H3 deacetylation. *CDH1* expression is suppressed as a consequence of the downregulated promoter activity. In this context, nuclear PKM2 serves as a transcriptional cofactor regulating TGIF2 behavior.

Few reports have investigated the significance of TGIF2 in cancer. In ovarian cancer, TGIF2 is reportedly amplified and overexpressed (22), whereas a comparison between colorectal adenoma and colorectal carcinoma revealed that TGIF2 expression is increased only in the latter (23). Further, TGIF2 has been shown to interact with TGF-β–activated SMADs and be able to repress the activation of TGF-β–responsive transcription (17). The present study demonstrated that TGIF2 affects *CDH1* expression through the regulation of promoter activity in which TGIF2 is supposed to function as an activating transcription factor.

TGF-β1 is a multifunctional cytokine that has dual and opposing roles in controlling cell fate. In the early stages of cancer, TGF-β1 induces growth arrest and apoptosis, exerting tumor-suppressive effects, whereas in later stages, TGF-β1 enhances tumor progression by provoking a variety of malignancy-related responses, including EMT (24–26). This paradox remains unsolved despite numerous studies addressing the issue. However, based on the results in the present study, we propose that the interaction between PKM2 and TGIF2 may offer a plausible explanation. In normal cells, PK expression is exclusively shifted to PKM1, but on TGF-β signaling, TGIF2 can suppress transcription downstream of the SMAD signal. Conversely, in cancer cells abundantly expressing PKM2, PKM2 translocates and is bound to TGIF2 in the nucleus, thereby reversing TGF-β signal transduction. Further investigation is necessary to determine the significance of TGIF2 expression and the precise mechanism underlying this interaction.

Nuclear PKM2 forms a dimer and functions as a protein kinase, whereas cytoplasmic PKM2 forms a tetramer and functions as a pyruvate kinase (15). In the present study, the dimeric form of PKM2 was increased, suggesting that the protein kinase activity of PKM2 is enhanced during EMT. PKM2 translocates into the nucleus in response to variable signals, of which, the EGF–ERK pathway is the most investigated (7, 27). Interestingly, TGIF2 is phosphorylated in response to EGF signaling (17). Given that EGF induces nuclear translocation of PKM2, PKM2 may function as a dimeric protein kinase in the

nucleus, phosphorylating TGIF2. However, the phosphorylation status of TGIF2 was not addressed in our study. Gao et al. (15) demonstrated that PKM2 interacts with STAT3 to control downstream gene expression in SW480 cells. Thus, it is conceivable that the molecular interaction of PKM2 is highly context dependent, with cell fate determined by how nuclear PKM2 regulates gene expression.

PKM2 has both metabolic and nonmetabolic functions, which are essential in the cytoplasm and nucleus, respectively. Increasing evidence has suggested that nuclear PKM2 binds to numerous transcriptional factors, thereby conferring cells with advanced malignant potential. The present study determined that PKM2 significantly influences EMT induction by modulating *CDH1* expression, thus providing a molecular basis for EMT acquisition. Future cancer treatments may be able to target the inhibition of nuclear PKM2.

Methods

Cell Lines and Culture. The human colorectal cancer cell lines, SW480 and HCT116, were obtained from ATCC, and CaR-1 was obtained from JCRB. These cell lines were grown in DMEM (Sigma-Aldrich) supplemented with 10% (vol/vol) FBS (Thermo Fisher Scientific), 100 U/mL penicillin, and 100 U/mL streptomycin (Life Technologies) and grown at 37 °C in a humidified incubator with 5% CO_2.

EMT Induction. Cells were seeded at a concentration of 5.0×10^4 cells/mL and incubated in a humidified atmosphere (37 °C and 5% CO_2) in standard medium for 48 h, after which they were treated with TGF-β1 (2.5 ng/mL; Sigma-Aldrich). Next, they were incubated with MEM supplemented with 10 ng/mL FBS-free EGF (Sigma-Aldrich), 100× insulin-transferring selenium (ITS; Life Technologies), and 50 nmol/L hydrocortisone (Tokyo Kasei) for 48–96 h.

ACKNOWLEDGMENTS. We thank the members of our laboratories for helpful discussions; Idea Consultants, Inc. (Osaka, Japan) and Olympus Co. (Tokyo, Japan) for technical assistance; Lewis C. Cantley for providing the lentiviral shRNA and retroviral expression vector; and H. Miyoshi for providing the packaging plasmids.

1. Jemal A, et al. (2011) Global cancer statistics. *CA Cancer J Clin* 61(2):69–90.
2. Warburg O (1956) On the origin of cancer cells. *Science* 123(3191):309–314.
3. Vander Heiden MG, Cantley LC, Thompson CB (2009) Understanding the Warburg effect: The metabolic requirements of cell proliferation. *Science* 324(5930):1029–1033.
4. Christofk HR, et al. (2008) The M2 splice isoform of pyruvate kinase is important for cancer metabolism and tumour growth. *Nature* 452(7184):230–233.
5. Hacker HJ, Steinberg P, Bannasch P (1998) Pyruvate kinase isoenzyme shift from L-type to M2-type is a late event in hepatocarcinogenesis induced in rats by a choline-deficient/DL-ethionine-supplemented diet. *Carcinogenesis* 19(1):99–107.
6. Elbers JR, et al. (1991) Pyruvate kinase activity and isozyme composition in normal fibrous tissue and fibroblastic proliferations. *Cancer* 67(10):2552–2559.
7. Yang W, et al. (2011) Nuclear PKM2 regulates β-catenin transactivation upon EGFR activation. *Nature* 480(7375):118–122.
8. Luo W, et al. (2011) Pyruvate kinase M2 is a PHD3-stimulated coactivator for hypoxia-inducible factor 1. *Cell* 145(5):732–744.
9. Hanahan D, Weinberg RA (2011) Hallmarks of cancer: The next generation. *Cell* 144(5):646–674.
10. Weinberg RA (2008) Mechanisms of malignant progression. *Carcinogenesis* 29(6): 1092–1095.
11. Rees JR, Onwuegbusi BA, Save VE, Alderson D, Fitzgerald RC (2006) In vivo and in vitro evidence for transforming growth factor-beta1-mediated epithelial to mesenchymal transition in esophageal adenocarcinoma. *Cancer Res* 66(19):9583–9590.
12. Yokobori T, et al. (2013) Plastin3 is a novel marker for circulating tumor cells undergoing the epithelial-mesenchymal transition and is associated with colorectal cancer prognosis. *Cancer Res* 73(7):2059–2069.
13. Okada H, Danoff TM, Kalluri R, Neilson EG (1997) Early role of Fsp1 in epithelial-mesenchymal transformation. *Am J Physiol* 273(4 Pt 2):F563–F574.
14. Strutz F, et al. (2002) Role of basic fibroblast growth factor-2 in epithelial-mesenchymal transformation. *Kidney Int* 61(5):1714–1728.
15. Gao X, Wang H, Yang JJ, Liu X, Liu ZR (2012) Pyruvate kinase M2 regulates gene transcription by acting as a protein kinase. *Mol Cell* 45(5):598–609.
16. Goldberg MS, Sharp PA (2012) Pyruvate kinase M2-specific siRNA induces apoptosis and tumor regression. *J Exp Med* 209(2):217–224.
17. Melhuish TA, Gallo CM, Wotton D (2001) TGIF2 interacts with histone deacetylase 1 and represses transcription. *J Biol Chem* 276(34):32109–32114.
18. Lugli A, Karamitopoulou E, Zlobec I (2012) Tumour budding: A promising parameter in colorectal cancer. *Br J Cancer* 106(11):1713–1717.
19. Ueno H, et al. (2014) Novel risk factors for lymph node metastasis in early invasive colorectal cancer: A multi-institution pathology review. *J Gastroenterol* 49(9):1314–1323.
20. Clower CV, et al. (2010) The alternative splicing repressors hnRNP A1/A2 and PTB influence pyruvate kinase isoform expression and cell metabolism. *Proc Natl Acad Sci USA* 107(5):1894–1899.
21. David CJ, Chen M, Assanah M, Canoll P, Manley JL (2010) HnRNP proteins controlled by c-Myc deregulate pyruvate kinase mRNA splicing in cancer. *Nature* 463(7279): 364–368.
22. Imoto I, et al. (2000) Amplification and overexpression of TGIF2, a novel homeobox gene of the TALE superclass, in ovarian cancer cell lines. *Biochem Biophys Res Commun* 276(1):264–270.
23. Lips EH, et al. (2008) Integrating chromosomal aberrations and gene expression profiles to dissect rectal tumorigenesis. *BMC Cancer* 8:314.
24. Roberts AB, Wakefield LM (2003) The two faces of transforming growth factor beta in carcinogenesis. *Proc Natl Acad Sci USA* 100(15):8621–8623.
25. Tian M, Schiemann WP (2009) The TGF-beta paradox in human cancer: An update. *Future Oncol* 5(2):259–271.
26. Rahimi RA, Leof EB (2007) TGF-beta signaling: A tale of two responses. *J Cell Biochem* 102(3):593–608.
27. Yang W, et al. (2012) ERK1/2-dependent phosphorylation and nuclear translocation of PKM2 promotes the Warburg effect. *Nat Cell Biol* 14(12):1295–1304.

Supporting Information

Hamabe et al. 10.1073/pnas.1407717111

SI Methods

shRNA Construct and Lentivirus Production. The shRNA construct was provided by Lewis Cantley (Harvard Medical School, Cambridge, MA) and cloned into the lentivirus vector pLKO. The oligonucleotide sequence of the shRNA targeting PK was 5′-CCGGGCTGTGGCTCTAGACACTAAACTCGAGTTTAGTGTCTAGAGCCACAGCTTTTTG-3′. The vector was cotransfected into 293T cells along with expression vectors containing the gag/pol, rev, and vs.vg genes. Lentivirus was harvested 48 h after transfection, and 5 μg/mL polybrene was added. SW480 cells were infected with harvested lentivirus and selected with 2 μg/mL puromycin for 1 wk.

Overexpression Constructs and Retroviral Production. Mouse PKM1 and PKM2 with FLAG peptide tags were cloned into the retroviral vector pLHCX (provided by Lewis Cantley, Harvard Medical School). The vectors were transfected into the Platinum-A Retroviral Packaging Cell Line (Cell Biolabs). The retrovirus was harvested 36 h after transfection, and 5 μg/mL polybrene was added. SW480 cells were infected with harvested retrovirus and selected with 600 μg/mL hygromycin for 2 wk.

Cross-Linking. For the cross-linking of PKM2 in nuclear extracts, SW480 cells were seeded into 10-cm dishes and cultured in normal conditions [DMEM supplemented with 10% (vol/vol) FBS], MEM supplemented with EGF alone, TGF-β1 alone, or EGF and TGF-β1 for 72 h each, and the above-described EMT induction method was applied. The cells were washed three times with PBS to remove serum proteins and then incubated on culture plates with a hypotonic buffer (PBS diluted by a factor of 10) for 15 min. After three washes with the hypotonic buffer, the cells were cross-linked with the homobifunctional *N*-hydroxysulfosuccinimide-ester cross-linker, DTSSP (Thermo Fisher Scientific) for 30 min, according to the manufacturer's protocol. The treated cells were lysed with an equivalent amount of concentrated RIPA buffer [50 mM Tris·HCl (pH 7.6), 300 mM NaCl, 1% Nonidet P-40] and successively quenched with 10 mM Tris·HCl for an additional 15 min. After centrifugation at 14,000 × *g* for 15 min, the supernatant was collected. For ChIP assays, sample tubes were placed in a floating rack and sonicated in an ultrasonic bath (Bransonic 2510) filled with iced water for 5 min. For the experiment analyzing the composition of the PKM2 complex, the cells were washed three times with PBS and cross-linked with the water-soluble, membrane-permeable, homobifunctional imidoester cross-linker dimethyl suberimidate (Thermo Fisher Scientific) for 30–60 min, according to the manufacturer's protocol.

Immunoprecipitation. Samples were subjected to immunoprecipitation using anti-PKM2, anti-TGIF2, and anti-acetylated H3K9 antibodies, and Protein G Mag Sepharose (GE Healthcare Biosciences) according to the manufacturer's protocol. The covalent bond was cleaved with 10 mM DTT, and eluates were subjected to each assay.

In-Gel Digestion and MS Identification of Proteins. In-gel digestion and MS identification of proteins were performed as described previously (1). The peptides were purified with ZipTip (Millipore Corporation) according to the manufacturer's protocol and analyzed using an Ultraflex tof/tof (Bruker Daltonics) MALDI mass spectrometer and MASCOT software (Matrix Science).

PCR. Total RNA was extracted from cultured cells using the RNeasy Mini Kit and QIAshredder (Qiagen). cDNA was synthesized with ReverTra Ace reverse transcriptase (TOYOBO Co.). Real-time quantitative PCRs (qRT-PCRs) were conducted with the LightCycler-FastStart DNA Master SYBR Green I Kit (Roche Applied Science). The primer sequences used in this study were: human *PK* sense, 5′-AGTACCATGCGGAGACCATC-3′; human *PK* antisense, 5′-GCGTTATCCAGCGTGATTTT-3′; human *PKM1* sense, 5′-TTGTGCGAGCCTCAAGTCACT-3′; human *PKM1* antisense, 5′-CTGACGAGCTGTCTGGGGAT-3′; human *PKM2* sense, 5′-TCCGCCGCCTGGCGCCCATTA-3′; human *PKM2* antisense, 5′-CTGACGAGCTGTCTGGGGAT-3′; human *CDH1* sense, 5′-ACACCATCCTCAGCCAAGA-3′; human *CDH1* antisense, 5′-CGTAGGGAAACTCTCTCGGT-3′; human *VIM* sense, 5′-TCCAGCAGCTTCCTGTAGGT-3′; human *VIM* antisense, 5′-CCCTCACCTGTGAAGTGGAT-3′; human *ZEB1* sense, 5′-TATGAATGCCCAAACTGCAA-3′; human *ZEB1* antisense, 5′-TGGTGATGCTGAAAGAGACG-3′; human *SNAI2* sense, 5′-TCAGCTCAGGAGCATACAGC-3′; human *SNAI2* antisense, 5′-GACTCACTCGCCCCAAAGA-3′; human *TGIF2* sense, 5′-GTGCTGTTTCTGTCAAGCCA-3′; human *TGIF2* antisense, 5′-AGCTCACCAGAACGCTATCA-3′; human *TGF-β1* sense, 5′-GAGCCCAAGGGCTACCAT-3′; human *TGF-β1* antisense, 5′-GTCCAGGCTCCAAATGTAGG-3′; human *ACTB* sense, 5′-GATGAGATTGGCATGGCTTT-3′; human *ACTB* antisense, 5′-CACCTTCACCGTTCCAGTTT-3′; mouse *SNAIL* sense, 5′-TCCAAACCCACTCGGATGTGAAGA-3′; mouse *SNAIL* antisense, 5′-TTGGTGCTTGTGGAGCAAGGACAT-3′; mouse *SLUG* sense, 5′-CACATTCGAACCCACACATTGCCT-3′; mouse *SLUG* antisense, 5′-TGTGCCCTCAGGTTTGATCTGTCT-3′; human *CDH1* promoter 1 sense, 5′-CTCATGGCTCACACCTGAAA-3′; human *CDH1* promoter 1 antisense, 5′-AGTACAGGTGCACACCACCA-3′; human *CDH1* promoter 2 sense, 5′-GCTTGGGTGAAAGAGTGAGC-3′; human *CDH1* promoter 2 antisense, 5′-TAGGTGGGTTATGGGACCTG-3′. Data were normalized to the expression of a control gene (β-actin) for each experiment. Data represent the mean ± SD of three independent experiments.

Genetic Recombination in Mouse Mesenchymal Cells. The *Pkm1* and *Pkm2* KI and KO were generated by homologous recombination of exon 9 with poly(A)-tailed cDNA to disrupt splicing to exon 10 [*Pkm1*KI adipocyte-derived mesenchymal cells (ADCs)] and by homologous recombination of exon 10 with poly(A)-tailed cDNA to disrupt splicing to exon 9 (*Pkm2*KI ADCs). The experimental protocol was approved by the Institutional Committee for Animal Use.

Western Blot Analysis. Total protein was extracted from the cell lines in radio immunoprecipitation assay (RIPA) buffer (Thermo Fisher Scientific). Nuclear and cytosolic protein were isolated using the Qproteome Nuclear Protein Kit (Qiagen) for cytosolic protein extraction and the Qproteome Mammalian Protein Prep Kit (Qiagen) for lysing the pellet of the nuclear fraction. Aliquots of protein were electrophoresed on SDS/PAGE Tris·HCl gels (Bio-Rad Laboratories). The separated proteins were transferred to polyvinylidene difluoride membranes using iBlot (Life Technologies) and incubated with primary antibodies overnight, followed by incubation with HRP-linked anti-rabbit or anti-mouse IgG (GE Healthcare Biosciences) at a dilution of 1:100,000 for 1 h at room temperature. The antigen–antibody complex was detected with the ECL Prime Western Blotting Detection Kit (GE Healthcare Biosciences). The intensity of the blots was quan-

tified by densitometry analysis using ImageJ software (National Institutes of Health, Bethesda, MD).

Antibodies. Antibodies specific to PKM1 (ABGENT, AP7476), PKM2 (Cell Signaling Technology, #4053), *CDH1* (Cell Signaling Technology, #3195), *VIM* (Cell Signaling Technology, #5741), and TGIF2 (Millipore, 09–718) for Western blot and immunoprecipitation, TGIF2 (Abcam, ab155948) for immunohistochemistry, histone H3 (Cell Signaling Technology, #9715), acetyl-histone H3 (Lys9) (Cell Signaling Technology, #9671), α-tubulin (Sigma-Aldrich, T9026), ACTB (Sigma-Aldrich, A2066), SMAD2 (Cell Signaling Technology, #3102), phospho-SMAD2 (Cell Signaling Technology, #3101), ERK (Cell Signaling Technology, #4695), phospho-ERK (Cell Signaling Technology, #4370), and normal rabbit IgG (Sigma-Aldrich, I5006) were used. In the immunoprecipitation assays with PKM2 antibody, three types of anti-PKM2 antibodies (Abcam, ab100841; Bethyl Laboratories, A303-659A; Bethyl Laboratories, A303-660A) were mixed in equal amounts and used.

RNA Interference. PKM2 and TGIF2 KD was carried out using siRNA oligonucleotides synthesized by Sigma-Aldrich. After 36 h in culture after seeding, siRNAs were transfected into SW480 cells at 20 nM final concentrations with Lipofectamine RNAiMax (Life Technologies), using a forward transfection method according to the manufacturer's protocol. EMT induction was initiated after 12-h incubation with siRNA, and the cells were harvested at the indicated times. The following sequence was used according to the report demonstrating the RNA sequence specifically targeting PKM2 (2): siControl, 5′-CUUACGCUGAGUACUUCGA-3′; siPKM2, 5′-CCAUAAUCGUCCUCACCAA-3′. siTGIF2 was purchased from Sigma-Aldrich (SASI_Hs01_00107440).

Cell Migration Assay. siRNAs were transfected into the SW480 cells at a final concentration of 10 nM with Lipofectamine RNAiMax (Life Technologies), and 24 h after transfection, 5×10^4 cells were seeded into each insert of a 24-well Biocoat Matrigel Invasion Chamber (BD Biosciences) in triplicate. FBS was added to a final concentration of 10% in the lower chambers to induce cell migration. After incubation for 72 h, the cells remaining above the insert membranes were carefully removed with cotton swabs, and the cells that had migrated to the other sides of the membranes were stained with the Diff-Quik Kit (Sysmex Corp.). The total number of migrated cells in three random microscopic fields were counted in each chamber.

Protein Study. Protein concentrations in these samples were measured using the Protein Assay System (Bio-Rad Laboratories). Aliquots containing 100 μg of proteins were applied overnight to an Immobiline Drystrip (GE Healthcare Biosciences) by in-gel rehydration (3, 4). The rehydrated gels were then gently dried with filter paper to remove excess fluid, and isoelectric focusing (IEF) was performed in a Pharmacia Hoefer Multiphor II electrophoresis chamber (GE Healthcare Biosciences) according to the manufacturer's instructions. SDS/PAGE was performed on 9–18% acrylamide gradient gels using an Iso-Dalt electrophoresis chamber. The gels were stained with SYPRO Ruby (Life Technologies) according to the manufacturer's protocol (5). The SYPRO Ruby-stained proteins were detected using the Molecular Imager FX (Bio-Rad Laboratories) and subjected to in-gel digestion. Image analysis and database management were carried out using Image Master Platinum software (GE Healthcare Biosciences).

Clinical Tissue Samples. Colorectal tissue samples ($n = 61$) were collected during surgery (2003–2009) in the Department of Gastroenterological Surgery, Osaka University. None of the patients had undergone preoperative chemotherapy or irradiation. Samples were fixed in buffered formalin at 4 °C overnight, processed through graded ethanol solutions, and embedded in paraffin. The specimens were appropriately used under the approval of the ethics committee at the Graduate School of Medicine, Osaka University.

Immunohistochemistry. Tissue sections (3.5 μm thick) were prepared from paraffin-embedded blocks. After antigen retrieval treatment in 10 mM citrate buffer (pH 6.0) at 115 °C for 15 min using Decloaking Chamber NxGen (Biocare Medical), immunostaining was performed using the Vectastain ABC Peroxidase Kit (Vector Laboratories). The slides were incubated overnight at 4 °C at the following dilution: PKM2 Ab, 1:800; E-cadherin Ab, 1:800; TGIF2 Ab, 1:200. The intensity at the deepest part of the tumor was evaluated in each sample. The deepest part of the tumor corresponded to the invasive front of the tumor that was defined as the tumor advancing edge (6–8).

Visualization of PKM2 Localization. SW480 cells were transiently transfected with PKM2 tagged with HaloTag cloned into pFN21A vector (Kazusa DNA Research Institute, FHC07869) using Fugene 6 Transfection Reagent (Promega). Expression levels of HaloTag–PKM2 fusion proteins were visualized by fluorescent labeling of the HaloTag protein using a HaloTag–TMR ligand (Promega). Nuclei were also labeled with Hoechst33342 according to a previously reported method (9). Photomicrographs were recorded using a laser confocal microscope (FV1000-D; Olympus Corporation).

Immunofluorescent staining for PKM2 quantification was performed according to the standard procedure. In brief, cells were fixed with 4% paraformaldehyde for 15 min at room temperature, membranes were made permeable with 0.3% Triton X-100, and the cells were blocked with 5% goat serum. The cells were then incubated with diluted PKM2 antibody (1:100) at 4 °C overnight and subsequently with Alexa Fluor dye-conjugated secondary antibody (Life Technologies). Nuclei were labeled with DAPI. Fluorescence intensity was quantified using Cellomics CellInsight (Thermo Fisher Scientific).

ELISA. CRC cells were seeded at 5×10^5 on 10-cm dishes. After 48 h of incubation, the medium was collected and the concentrations of TGF-β1 were detected by ELISA using the TGF-β1 Quantikine ELISA Kit (R&D Systems) according to the manufacturer's protocol. Medium containing 10% (vol/vol) FBS was used to measure the background signal.

Gene Expression Dataset. A gene expression dataset of primary colorectal tumors (accession no. GSE17536) was downloaded from the Gene Expression Omnibus database (10).

1. Kristensen DB, Imamura K, Miyamoto Y, Yoshizato K (2000) Mass spectrometric approaches for the characterization of proteins on a hybrid quadrupole time-of-flight (Q-TOF) mass spectrometer. *Electrophoresis* 21(2):430–439.
2. Goldberg MS, Sharp PA (2012) Pyruvate kinase M2-specific siRNA induces apoptosis and tumor regression. *J Exp Med* 209(2):217–224.
3. Rabilloud T, Valette C, Lawrence JJ (1994) Sample application by in-gel rehydration improves the resolution of two-dimensional electrophoresis with immobilized pH gradients in the first dimension. *Electrophoresis* 15(12):1552–1558.
4. Sanchez JC, et al. (1997) Improved and simplified in-gel sample application using reswelling of dry immobilized pH gradients. *Electrophoresis* 18(3-4):324–327.
5. Lopez MF, et al. (2000) A comparison of silver stain and SYPRO Ruby Protein Gel Stain with respect to protein detection in two-dimensional gels and identification by peptide mass profiling. *Electrophoresis* 21(17):3673–3683.
6. Del Casar JM, et al. (2009) Comparative analysis and clinical value of the expression of metalloproteases and their inhibitors by intratumor stromal fibroblasts and those at the invasive front of breast carcinomas. *Breast Cancer Res Treat* 116(1):39–52.

7. Vignjevic D, et al. (2007) Fascin, a novel target of beta-catenin-TCF signaling, is expressed at the invasive front of human colon cancer. *Cancer Res* 67(14):6844–6853.
8. Ono M, et al. (1996) Cancer cell morphology at the invasive front and expression of cell adhesion-related carbohydrate in the primary lesion of patients with colorectal carcinoma with liver metastasis. *Cancer* 78(6):1179–1186.
9. Nagase T, et al. (2008) Exploration of human ORFeome: High-throughput preparation of ORF clones and efficient characterization of their protein products. *DNA Res* 15(3):137–149.
10. Smith JJ, et al. (2010) Experimentally derived metastasis gene expression profile predicts recurrence and death in patients with colon cancer. *Gastroenterology* 138(3):958–968.

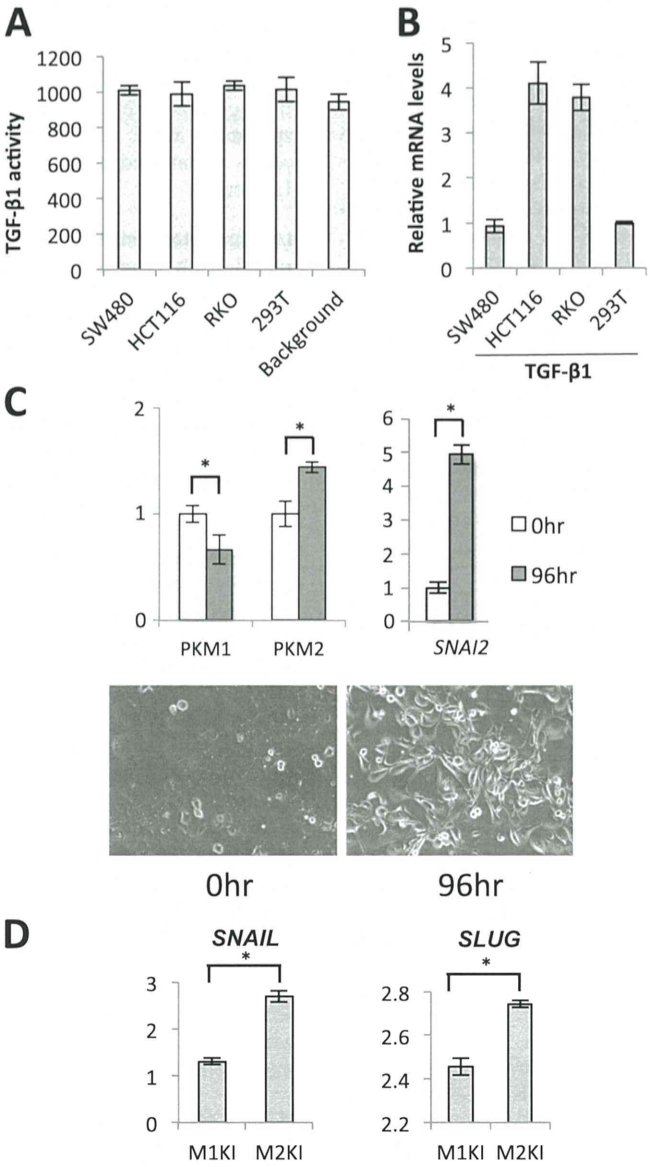

Fig. S1. mRNA expression and protein secretion of TGF-β1 from CRC cells. (*A*) TGF-β1 secreted from CRC cells in the medium measured by ELISA. (*B*) mRNA expression of TGF-β1 was studied in CRC cells. The data indicate that TGF-β1 expression and secretion was not significantly increased in the SW480 cells that we used, suggesting that endogenous TGF-β1 was unlikely to affect the present observations. (*C*) The EMT induction in human colorectal cancer CaR-1 cells. Cells were cultured in the medium with EGF and TGF-β1, and RNA was extracted. The qRT-PCR indicated that the PKM2 expression was increased (graph), and the spindle-shaped phenotypes were induced in EMT condition (photos, ×200). (*D*) Expression of *SNAIL* and *SLUG* in mesenchymal cells from *Pkm1*KI (*Pkm2*-deficient) and *Pkm2*KI (*Pkm1*-deficient) mice. The qRT-PCR results indicated that mouse *SNAIL* and *SLUG* expression was increased in *Pkm2*KI cells, compared with *Pkm*1KI cells, suggesting that *Pkm2* plays a role in the acquisition of mesenchymal phenotypes. $*P < 0.01$.

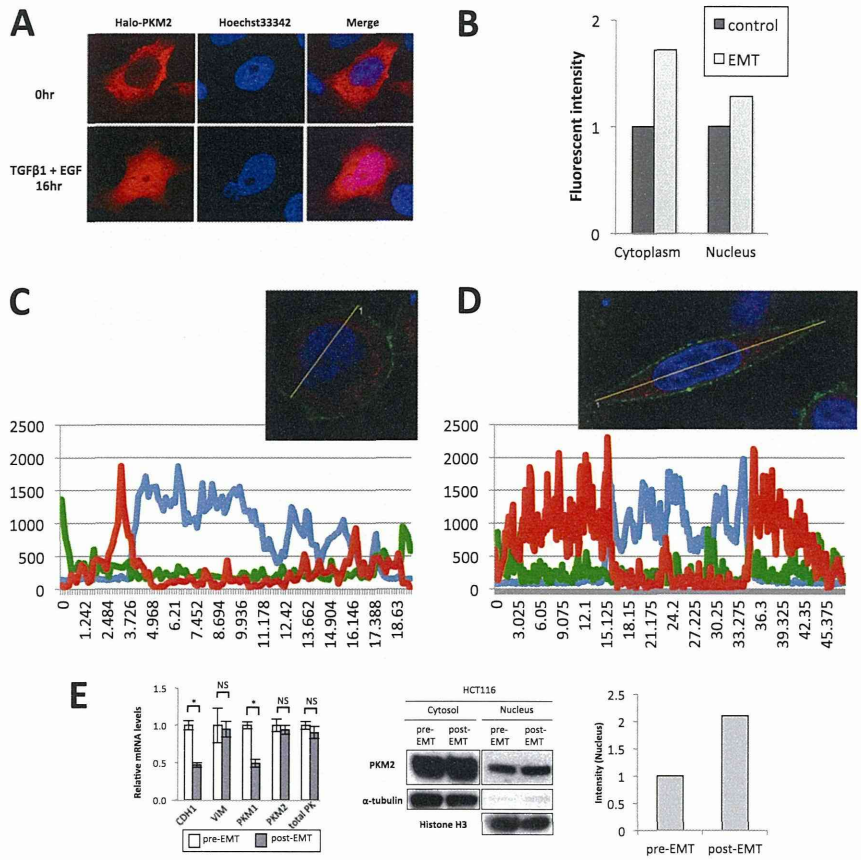

Fig. S2. Pkm2 translocates into the nucleus during EMT. (*A*) PKM2 tagged with HaloTag was labeled with the TMR ligand, followed by EMT induction (5 ng/mL TGF-β1 + 10 ng/mL EGF) for 16 h. (*B*) Quantification of PKM2 in the cytosol and nucleus according to immunofluorescence intensity analysis. (*C* and *D*) Nuclear translocation of PKM2 was assessed before (*C*) and after (*D*) treatment with EGF and TGF-β1 using a laser scanning microscope (FV1200-IX83; Olympus), equipped with a glass objective (UPLSAPO60×S; Olympus). Excitation wavelengths were 405, 473, and 559 nm. The primary mouse mAb against E-cadherin (Cell Signaling Technology #5296) was detected by the secondary FITC-conjugated anti-mouse IgG (H+L), F(ab)2 Fragment (Green color; Cell Signaling Technology #4408). Expression levels of HaloTag–PKM2 fusion proteins were visualized by fluorescent labeling of the HaloTag protein using a HaloTag–TMR ligand (Red color; Promega). DAPI Solution (Dojindo 340–07971) was used to stain nuclei. The *x* axis denotes the distance along the longitudinal line of cells (μm), and the *y* axis shows the signal intensity (arbitrary units). Note that the increased PKM2 signal (red) is observed in the nuclear region (blue) of spindle-like cells (*D*). (*E*) EMT induction (TGF-β1 5 ng/mL plus EGF 10 ng/mL) in HCT116 cells. The qRT-PCR (*Left*) shows the reduction of *CDH1*; the PKM1 was reduced, suggesting a shift to PKM2. The Western blot shows the nuclear PKM2 (*Center*), and the ratios of nuclear PKM2 are demonstrated in EMT-inducing condition (*Right*).

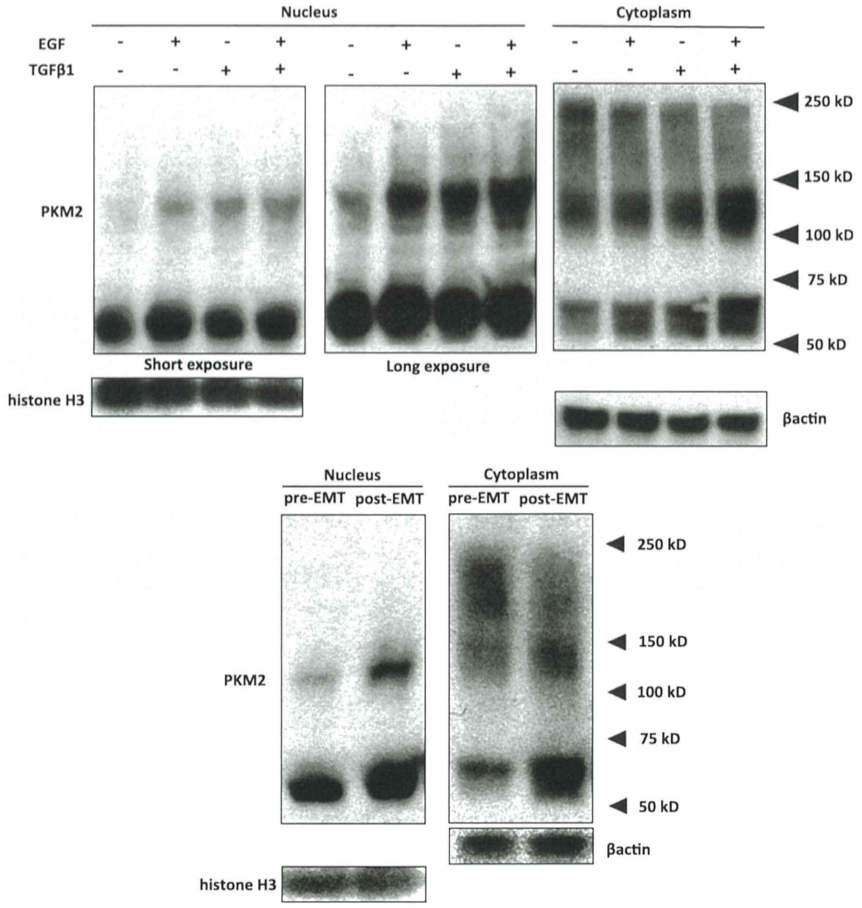

Fig. S3. Western blot analysis of nuclear and cytoplasmic proteins using anti-PKM2 antibody. SW480 cells were cultured in medium containing EGF and TGF-β1 (EMT-inducing condition) and treated with a cross-linker. The PKM2 bands with low mobility indicate tetramer formation in the cytoplasm but not in the nucleus. Dimer formation in the nucleus was increased after exposure to EGF and TGF-β1. Briefly, cytoplasmic fractions were treated with 1% formaldehyde for 10 min, and nuclear pellets were treated with 4 mg/mL dimethyl suberimidate for 60 min. Samples were lysed with equivalent amount of 2× RIPA buffer [50 mM Tris·HCl (pH 7.6), 300 mM NaCl, 1% Nonidet P-40, 2.5 U/mL Benzonase). SDS was added (a final concentration, 1%). After centrifugation at 14,000 × *g* for 15 min, supernatants were subjected to SDS/PAGE.